ACS APPLIED NANO MATERIALS

www.acsanm.org Article

Physicochemical Modulation of Nanometer-Thick Etalon Films for Liquid-Sensitive Color Display with Full-Color Spectrum Generation

Hee-Dong Jeong, Jongsu Lee, Eui-Sang Yu, Taehyun Kim, In Soo Kim, Sin-Doo Lee, Yong-Sang Ryu,* and Seung-Yeol Lee*

Cite This: *ACS Appl. Nano Mater.* 2021, 4, 389−395 Read Online

ACCESS | Metrics & More | Article Recommendations | Supporting Information

ABSTRACT: Light−matter interactions based on noble metal nanostructures have received continued attention for their tremendous potential for the discovery of basic science as well as their application in practical devices driven by their unique optical characteristics. However, constructing such nanostructured platforms requires relatively expensive and complicated fabrication processes to produce a wide range of colors in the visible region. In this paper, we propose a simple nanoscale Fabry−Perot film capable of providing full-color coverage in the visible region with a high level of color tunability through engineering the geometries of the constituent layers. Specifically, the thicknesses and filling-fractions of each layer were precisely tailored to allow for fine color tuning together with theoretical modeling to set up a standard guideline of structural colors depending on such physical variables. The physicochemical property-dependent coloration was demonstrated via the simple nanometer-thick Fabry−Perot stack, which was further applied to functional mimicry of environmental sensitive optical camouflage.

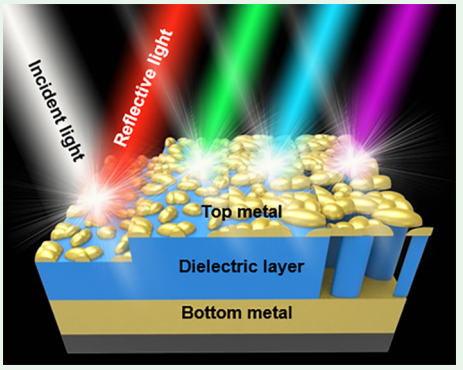

KEYWORDS: *structural color, metamaterials, thin-film resonator, color tuning, optical camouflage, nanostructured sensor*

Downloaded via RUTGERS UNIV on May 15, 2021 at 11:12:40 (UTC).
See https://pubs.acs.org/sharingguidelines for options on how to legitimately share published articles.

INTRODUCTION

Structural colors refer to the production of color by utilizing interference, absorption, and scattering of light from a wavelength or subwavelength scale nanostructures without the use of dyes or pigments. Such coloration behavior has been observed numerously in nature, such as in the wings of Morpho butterflies and the skin of chameleons[1] or in ancient human history, such as in the color of Roman Lycurgus cup and stained glass of the Middle Ages.[2] For a few decades, researchers have strived for implementing various methods to realize structural colors owing to their unique advantages including long-term stability, high reliability, efficient manipulation of visible light, and harmlessness to the human body.[3] Diffraction gratings, selective mirrors, photonic crystals, and deformed matrices[4,5] have been widely employed and continuously developed to achieve structural colors in a variety of research fields, such as bio/chemical sensors, color filters, absorbers, anticounterfeiting stickers, and optical camouflage devices.[6−11]

Fabricating micro/nanoscale structures for structural colors via top-down processes is inherently disadvantageous in industrial aspects due to its high complexity and costs which clearly limits scalability and thus mass production. On the other hand, bottom-up processes may resolve such issues in achieving structural colors through simple deposition processes or spreading of randomly distributed metal nanoparticles/nanowires at subwavelength scales.[12−14] In this aspect, a device that confines specific wavelengths of incident light within a metal−dielectric−metal (MDM) stack demonstrated unique opportunities in color displays by taking advantage of an optical phenomenon called Fabry−Perot (FP) resonance or Mie scattering.[15−20] In addition, a color modulator using enhanced Mie scattering with lattice resonance has also been reported.[21] Previously, we demonstrated a reflective liquid-permeable MDM etalon for the refractive index (RI) sensor working in the visible region with a record high color shift value of 323.5 nm/RIU, depending on the RI of the infiltrated solution.[14] However, an achievement of high level of color tunability without covering the full-colored visible range is insufficient to satisfy its availability for practical real-world application. Besides, establishment of a color guide map of MDM stack with delicate control of its constituents is highly desirable.

Here, we report a full spectrum of structural colors with a nanometer-thick FP etalon film consisting of a uniform film of transreflective gold (Au), perfluoro-(butenyl vinyl ether) (PBVE) polymer dielectric film, and bottom reflective Au

Received: October 14, 2020
Accepted: December 10, 2020
Published: December 24, 2020

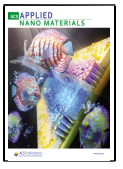

© 2020 American Chemical Society

https://dx.doi.org/10.1021/acsanm.0c02746
ACS Appl. Nano Mater. 2021, 4, 389−395

from the top to bottom. The roles of geometrical features of each layer on the device's coloration were examined by varying their thickness and filling fraction (i.e., top Au and PBVE films). Based on theoretical modeling coupled with experimental verification, we established color guide maps of the MDM etalon, which was further applied to functional mimicry of optical camouflage for environmental sensitive color display.

EXPERIMENTAL SECTION

MDM Etalon Fabrication. The bottom reflection layer was prepared by depositing a 10 nm titanium (Ti) adhesion layer followed by a 100 nm Au film on a silicon (Si) substrate using a thermal evaporator (MHS-1800, Muhan; 10^{-7} Torr; 2.0 Å/s). Dielectric films with various thicknesses (d = 110, 135, and 165 nm) were achieved by spin coating the mixture solution [9.0 wt % PBVE polymer (Chromis Technologies) in a fluoro solvent (FC-43, Chromis Technologies) in a ratio of 1:1] at controlled spinning rates (7200, 4400, and 3000 rpm for 45 s, respectively), followed by a baking process on a hotplate at 80 °C for 1 h. The thickness of PBVE was locally reduced using a reactive ion etcher (RIE 80 Plus, Oxford Instruments), and its surface energy was relieved by annealing on a hotplate at 180 °C for 2 h. O_2 plasma surface treatment (CUTE plasma system, Femto Science; 500 mTorr pressure, plasma generating frequency of 50 kHz, RF power of 70 W, and O_2 gas flow rate of 30 sccm) was performed on the PBVE surface to obtain high surface energy. The Bruggeman effective medium geometry of the top Au layer was slowly deposited on PBVE (10^{-7} Torr, 0.3 Å/s). Finally, additional dry etching was performed to create a dielectric cavity. More detailed fabrication steps of the discus fish sample is provided in Figure S1.

Reflectance Spectrum Measurement. Guided through an optical fiber reflection probe (R400-7-SR, Ocean Optics), white light from a deuterium and tungsten-halogen light source (DH-MINI, Ocean Optics) was incident on the sample in a normal direction. Then, normally reflected light was guided into ultraviolet−visible spectroscopy (USB4000-UV-VIS, Ocean Optics) with its spectral measurement ranging from 200 to 850 nm. During the measurements, reflectance spectra were normalized using an aluminum standard mirror (STAN-SSH, Ocean Optics). More detailed measurement setup is provided in Figure S2.

RESULTS AND DISCUSSION

The proposed MDM etalon reflects a wide range of colors depending on the physical properties of comprising films, such as dielectric layer (PBVE) thickness (t_{PBVE}), and volume filling fractions of the top metal (f_{Au}) and the dielectric layer (f_{PBVE}). To test the proposed concept of optical color variation, an MDM stack consisting of a 100 nm thick Au on a Si substrate (as a full reflector), PBVE polymer layer (as an optical cavity), and mixed Au/air top layer (as a transreflective metal film) was prepared beginning with 100 nm thick Au at the bottom. A low density nucleation of Au on the dielectric surface results in a randomly distributed mixed Au/air layer producing a controlled value of f_{Au}, by varying the deposition conditions such as time, rate, and pressure or the surface energy of the dielectric layer.[14,20] Throughout the paper, the influence of physicochemical properties of both top Au and PBVE layers on structural color generation of the MDM etalon will be examined.

Instead of solving the full electromagnetic equation of the proposed randomly distributed configuration, transfer matrix method (TMM) solution for a simplified one-dimensional multiple thin film stacked model was applied. The mixed Au/air layer was assumed as a homogeneous effective medium based on Bruggeman's effective medium theory (BEMT) which gives an effective permittivity of random mixtures consisting of two discrete materials with a subwavelength-scale morphology. The effective permittivity can be achieved by solving the following equation

$$f_1 \frac{\varepsilon_1 - \varepsilon_{mix}}{\varepsilon_1 + \kappa\varepsilon_{mix}} + f_2 \frac{\varepsilon_2 - \varepsilon_{mix}}{\varepsilon_2 + \kappa\varepsilon_{mix}} = 0 \quad (1)$$

Here, ε_i (i = 1, 2) and f_i (i = 1, 2) are the permittivity and the volume filling fraction of each constituent material in the mixture, respectively. κ is Lorentz depolarization factor, where κ = 1 for two-dimensional mixtures and κ = 2 for three-dimensional mixtures.[23] In our case, κ = 1 since the thickness of the layer is much smaller than the optical wavelength in the visible range. Thus, the proposed MDM structure may be regarded as thin-film multilayers (as a FP etalon), which can be interpreted by a simple TMM-based calculation.

To examine the influence of mixed Au/air layer in color tunability, color maps as a function of f_{Au} and t_{Au} were generated with select cases verified both theoretically and experimentally. In particular, Figure 1a shows four cases of

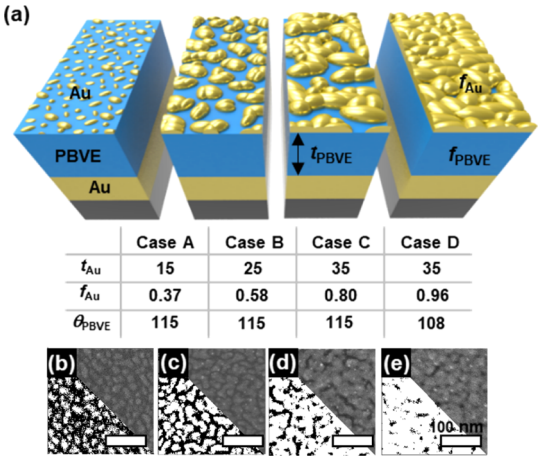

	Case A	Case B	Case C	Case D
t_{Au}	15	25	35	35
f_{Au}	0.37	0.58	0.80	0.96
θ_{PBVE}	115	115	115	108

Figure 1. (a) Schematic of MDM structures composed of Si substrate, 100 nm thick reflective Au film, PBVE, and Au/air mixture layer in bottom to top order. The condition of top Au/air layer was varied from cases A to D, and their values of t_{Au}, f_{Au}, and corresponding θ_{PBVE} are listed in the table below. (b−e) Top view SEM images of the top Au/air mixed layers from cases A to D, respectively.

MDM samples prepared by varying metal deposition conditions [identical values of deposition rate: 0.3 Å/s, chamber pressure: 10^{-7} Torr, the contact angle of 10 μL deionized (DI) water droplet on PBVE surface, and θ_{PBVE}: ∼115° while the deposition time varies for cases A−C]. The top view of the scanning electron microscopy (SEM) images confirmed that low density nucleation of Au on the hydrophobic PBVE surface created a particle-like Au layer with different t_{Au} and f_{Au} values (Figure 1b−e). For case D, the surface energy of PBVE was increased via O_2 plasma treatment, which in turn increased f_{Au} (θ_{PBVE}: ∼108°) while maintaining identical t_{Au} as case C (Figure 1e and Supporting Information S3). The results clearly demonstrate that controlled deposition conditions, such as deposition time (cases A−C) and underlying surface energy (case D), yield different f_{Au} and t_{Au}.

Based on the values obtained from experiments, numerical simulations were conducted using BEMT model to investigate the influence of physical parameters (i.e., f_{Au}, t_{Au}, and t_{PBVE}) on the coloration of each MDM configuration. Figure 2a−c illustrates the calculated reflective colors where f_{Au} ranges from

https://dx.doi.org/10.1021/acsanm.0c02746
ACS Appl. Nano Mater. 2021, 4, 389−395

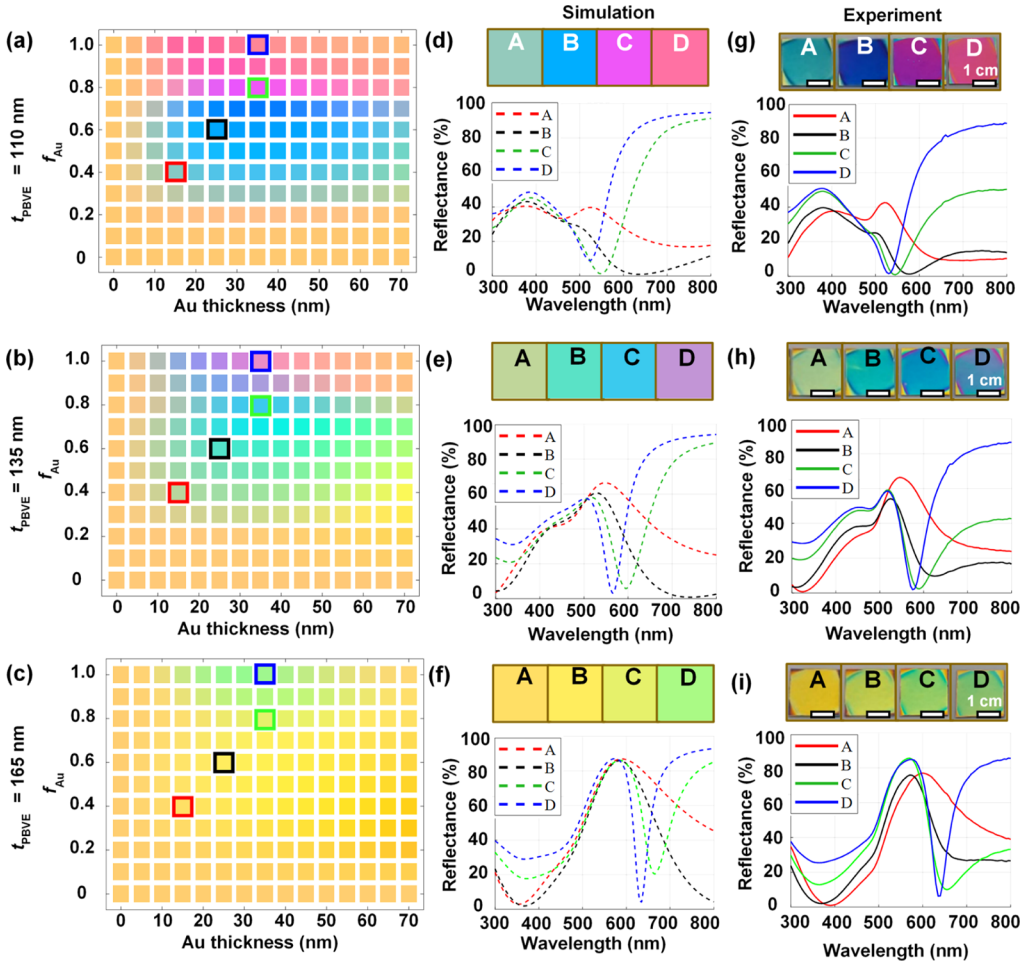

Figure 2. (a–c) Simulated reflective color maps of the MDM etalon with (a) 110, (b) 135, and (c) 165 nm t_{PBVE}, depending on various Au/air mixed layer condition. Variables, f_{Au} and t_{Au}, are swept from 0 to 1.0 with 0.1 interval and from 0 to 70 nm with 5 nm interval, respectively. Each color box indicates different Au/air mixed layer conditions (red: case A; black: case B; green: case C; and blue: case D). (d–f) Simulated reflectance spectra and extracted colors for the corresponding color boxes marked on (a–c) in the same row. (g–i) Experimentally measured reflectance spectra of the fabricated etalon samples (photographs on top; scale bars: 1 cm).

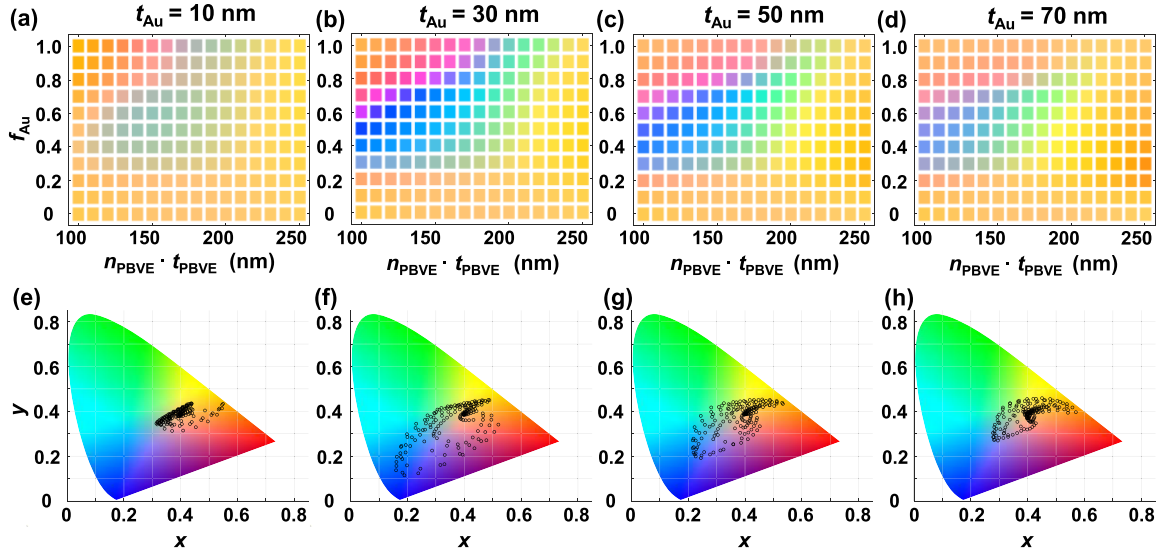

Figure 3. (a–d) Simulation results of colors that can be obtained by changing the structural condition of the proposed etalon. In each figure, the structural condition is that f_{Au} is changed from 0 to 1.0 with 0.1 interval and the optical path length of PBVE layer ($n_{PBVE} \cdot t_{PBVE}$) is changed from 100 to 250 nm with 10 nm interval at a fixed t_{Au} of (a) 10, (b) 30, (c) 50, and (d) 70 nm. (e–h) CIE1931 color maps with marks of all colors obtained from (a–d) in the same column.

https://dx.doi.org/10.1021/acsanm.0c02746
ACS Appl. Nano Mater. 2021, 4, 389–395

0 to 1 and t_{Au} from 0 to 70 nm when t_{PBVE} is 110, 135, and 165 nm, respectively. The result indicates that $f_{Au} < 0.2$ is incapable of producing variations in structural colors implying that the reflective colors under low $f_{Au} < 0.2$ are insufficient to yield color variations due to high portion of light transmission, losing its identity as an etalon. Thus, the reflective color from the bottom Au film is dominantly observed due to the transparency of PBVE. To verify the accuracy of the simulation model, the calculated reflection spectra and the corresponding colors (Figure 2d−f) were directly compared with the experimental results (Figure 2g−i). Additional color comparison on CIE1931 color space is provided in Figure S4.

By comparing Figure 2g−i, we observe that the increase in t_{PBVE} directly red-shifts the FP resonance (FPR) conditions, which is predicted by the Airy formula for thin-film interference. Hence, the location of FPR can be arbitrarily designed by precisely tuning t_{PBVE}. Then, the spectral variations in cases A−D suggest that f_{Au} is strongly correlated to the sharpness and location of the FPR dip, which becomes narrower and blue-shifted. All of these observations can be explained by varying the effective permittivity in the mixed Au/air layer. As the f_{Au} increases, the layer becomes more metallic causing an increase in the imaginary part of effective permittivity. This essentially increases reflections inside the etalon, which means that the *Q*-factor of MDM etalon becomes larger so that the FPR dip becomes stronger and sharper. Moreover, variations in the effective permittivity of mixed Au/air layer affect the phase of reflection coefficient between PBVE and mixed Au/air layers, resulting in the shift of the resonant wavelength condition.

In Figure 2c, it is worth noting that the color variation becomes subtle when t_{PBVE} = 165 nm compared with when t_{PBVE} = 110 nm or t_{PBVE} = 135 nm. Such optical behavior is attributed to the shift in the resonant wavelength of the etalon from the visible to the infrared band (Figure 2f,i). When $f_{Au} <$ 0.8, the FPR dip becomes much broader than the film-like top layer, and thus, wider FPR dips are expected to appear in the infrared band barely inducing visible color variation. On the other hand, in the case of $f_{Au} > 0.8$, a sharp resonance dip in the wavelength range near 630 nm is observed. As a consequence, the proposed etalon displays green color by absorbing the red spectrum.

Having established the roles of f_{Au} and t_{PBVE} in the generation of structural colors, we now investigate the role of t_{Au} with respect to color coverage. Figure 3a shows the simulated structural colors as a function of f_{Au} and the optical path length of PBVE layer (n_{PBVE}·t_{PBVE}), the values of which range from 0 to 1 and from 100 to 250 nm at t_{Au} = 10 nm, respectively. Similarly, Figure 3b−d displays the color guide maps via the proposed MDM etalon when t_{Au} = 30, 50, and 70 nm, respectively. Direct comparison of the color guides indicates that the hue of colors are mainly determined by the variation of f_{Au} and the optical path length of the PBVE layer, but the color saturation seems to have an optimized value determined by t_{Au}. To quantify this optical property, the CIE1931 color space was adopted, onto which the resultant colors from the color maps were marked (Figure 3e−h). From the results, the widest range of color variation as well as most distinguishable color change is expected at t_{Au} = 30 nm. It is also shown that for thinner top Au layers (Figure 3a), the transmission of incident light is more dominant than the reflection and thus leads to higher probability of Au-like color appearance compared to MDM etalons having thicker top Au layers (Figure 3b−d). The thicker the top Au becomes, the more the light is reflected and the higher the portion of FPR occurs in the optical cavity. The color guides (Figure 3a−d) and distribution of color marks (Figure 3e−h) suggest that the optimum thickness for distinguishing color variations is found near t_{Au} = 30 nm.

In contrast to other MDM etalons that completely passivate the dielectric layer with a top metal film, the proposed structure allows for tailoring of the underlying PBVE layer via reactive ion etching (RIE) through the nanoscale apertures of the top Au layer (Figure 4a). Since the upper Au layer

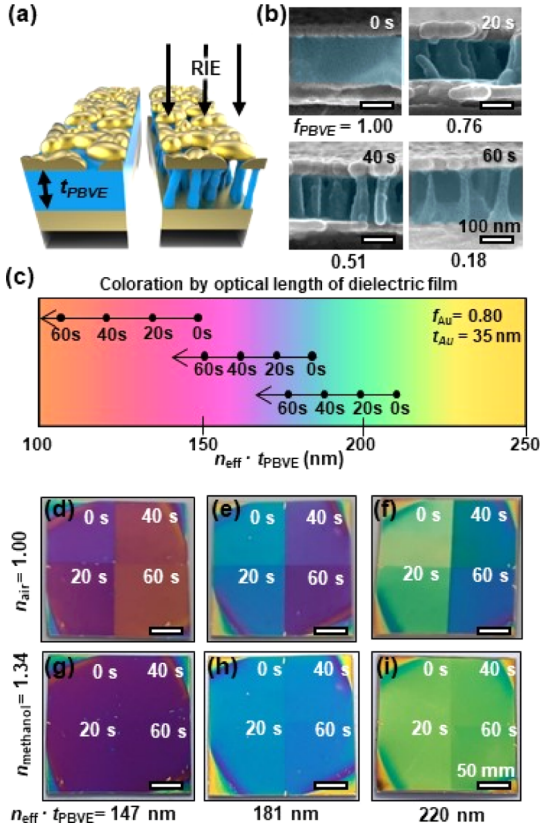

Figure 4. (a) Schematic cross section of a MDM etalon before and after RIE. (b) Cross-sectional SEM images of the etalon samples with different f_{PBVE} (1.00, 0.7, 0.51, and 0.18) for varying etching times (0, 20, 40, and 60 s, respectively). Note the dielectric layer is pseudo colored for clear recognition. (c) Simulated color map of the proposed structure depending on n_{eff}·t_{PBVE} where f_{Au} = 0.80 and t_{Au} = 35 nm. Indicated marks represent the color change by corresponding RIE etching times. (d−i) Photographs of the fabricated samples with different n_{eff}·t_{PBVE} and etching times (d−f) in air (n_{air} = 1.0) and (g−i) in methanol ($n_{methanol}$ = 1.34).

functions as a mask, this unique feature offers an opportunity to manipulate structural colors in a controlled manner. Figure 4b shows cross-sectional images of the samples which have undergone 0, 20, 40, and 60 s of RIE with resulting f_{PBVE} values of 1.00, 0.76, 0.51, and 0.18, respectively. The physicochemical properties of the dielectric layer mixed with PBVE nanopillars and air can also be modeled as a homogeneous layer through BEMT, analogous to the mixed Au/air films. Such additional etching procedures on the PBVE layer lowers its permittivity close to air, reducing its optical path length and imparting liquid permeability to the device since the effective RI of etched PBVE layer (n_{eff}) gradually

https://dx.doi.org/10.1021/acsanm.0c02746
ACS Appl. Nano Mater. 2021, 4, 389−395

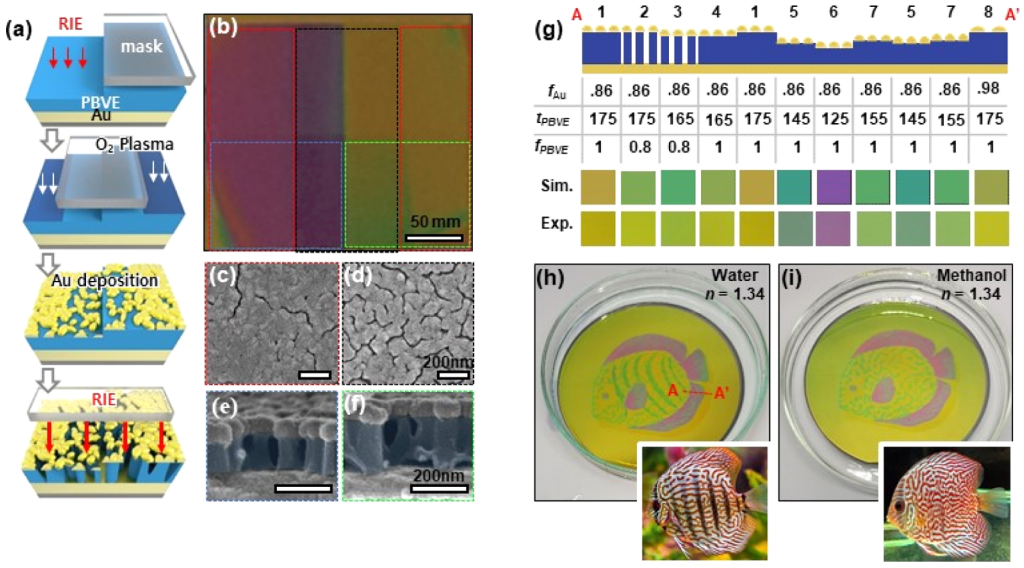

Figure 5. (a) Schematic description of the sample fabrication process. (b) Photograph of the resulting sample. (c–f) SEM images showing the top surfaces of dashed red box area and dashed black box area and cross sections of dashed blue box area and dashed green area from (b), respectively. (g) Schematic cross-sectional layer information of the discus fish demonstration sample with measured f_{Au}, t_{PBVE}, and f_{PBVE} followed by corresponding simulated colors and observed microscopic images. (h,i) Photographs of the demonstration sample in air (n_{air} = 1.00) and methanol ($n_{methanol}$ = 1.34) with insets showing photographs of a real-world discus fish with/without stripes (left/right, respectively). The red dashed line represents the cross-sectional position of (g).

decreases from n_{PBVE} = 1.34 to n_{air} = 1 (where n refers to the RI of the material in its subscript) based on the relation made by eq 1 and the subscript material. Figure 4c shows the simulated color change depending on n_{eff}·t_{PBVE} at f_{Au} = 0.80 and t_{Au} = 35 nm. Three arrows pointing to the left represent cases where n_{eff}·t_{PBVE} is 147, 181, and 220 nm each and their corresponding color shifts by RIE. It is shown that increasing the etching time results in the shortening of the effective t_{PBVE}. Figure 4d–f shows the experimental colors of the MDM etalons which were divided into four differently etched regions with etching periods of 0, 20, 40, and 60 s. Color matching between the simulated (Figure 4c) and measured data (Figure 4d–f) confirmed that infiltration of air into the PBVE layer tunes the dielectric property of the device. Now the etched etalons were immersed into methanol ($n_{methanol}$ = 1.34) to test additional color tuning of the etched regions to be matched with the nonetched PBVE (n_{PBVE} = 1.34) regions (Figure 4g–i). Such an optical camouflage phenomenon can be explained by the infiltration of index matching solvent to the hollow area of the dielectric layer.[14]

Through all of these variables for generating a wide range of structural colors, multiple colors were tested on a single MDM etalon sample through a series of surface energy modification technique together with dielectric etching processes prior/post to the top metal deposition for dielectric change of optical path length controls (Figure 5a). After establishment of the color guidelines via control of the physical factors (f_{Au}, f_{PBVE}, t_{Au}, and n_{eff}) of the etalon, the color properties were applied for "information encryption" using the optical camouflage. To make a thickness difference of the PBVE layer, the bulk PBVE film was spatially etched with controlled etching prior to the top Au deposition, followed by an additional annealing at 180 °C (above the glass transition temperature of PBVE, 108 °C), which is known to restore the original surface energy of PBVE after the RIE process (see Figures S1 and S3 for details).[22] Next, O_2 plasma mildly enhanced the surface energy of the red dashed boxed area in Figure 5b, resulting in f_{Au} of 0.98 after Au deposition (Figure 5c), whereas the black dashed region shaded by a mask produced f_{Au} of 0.86 (Figure 5d). Finally, the bottom half of the sample was exposed to additional RIE to form dielectric air pockets. Figure 5e,f obviously shows the PBVE nanopillars with different thicknesses (blue dashed region with t_{PBVE} = 165 nm, while green one with t_{PBVE} = 175 nm). Moving forward, this technique was applied to a more complicated layer configuration of MDM etalon to demonstrate the functional mimicry of discus fish whose appearance is changed in response to the changes in the environmental conditions.

Figure 5g shows 8 different sections with different structures and corresponding layer information, simulated colors, and experimental colors used to visualize a discus fish pattern (see detailed fabrication process in Figure S1). The resulting sample in Figure 5h has vertical line patterns in the body region, inspired by the camouflage ability of the discus fish to blend in with its surrounding tree roots (left inset). The cross section of the red dashed line (Figure 5h) follows the order (A to A′) of the schematic structure in Figure 5g. Interestingly, the proposed etalon shows highly sensitive infiltration characteristics according to the surface tension of the solution. While water (n_{water} = 1.34) on the fish-patterned sample did not show any distinguishable change, the vertical patterns disappeared when it was immersed in methanol ($n_{methanol}$ = 1.34) (Figure 5i) which even has the same RI value of water but affects much more and is environmentally hazardous to the ecosystem. Such demonstration of environmental sensitive structural color change (for more information, see Figure S5 in Supporting Information) based on selective liquid infiltration into the air pockets of the PBVE layer emphasizes the advantages of the proposed MDM etalon which is prepared based on the physicochemical understanding of the fabrication procedures.

https://dx.doi.org/10.1021/acsanm.0c02746
ACS Appl. Nano Mater. 2021, 4, 389–395

CONCLUSIONS

Through understanding of physical variables of the MDM etalon for the generation of structural colors, a wide spectrum of colors can be realized in a single device utilizing nanostructures over a large area with simple and scalable fabrication processes. Since the thickness variation of the transparent dielectric layer itself is incapable of showing visible color difference without the existence of the top Au layer, the proposed technique can be applied for multichromatic image encryption as well as simple message encryption by utilizing FPR (see examples in Figures S1 and S5). Also, its liquid permeability through the dielectric cavity makes it useful for real-world applications not only in a RI sensor but also in the demonstration of an optical camouflage with fast response and reproducibility. The comprehensive liquid-sensitive characteristics of the MDM etalon, which can not only be tuned through RI but also surface tension, can be used as various routes of optical coloration applications, such as environment-sensitive smart mirrors, humidity sensors, and other smart display techniques. Moreover, the proposed structure can be applied to the liquid-sensitive anticounterfeiting displays or optical camouflage displays to deliver hidden information for security purposes.

ASSOCIATED CONTENT

Supporting Information

The Supporting Information is available free of charge at https://pubs.acs.org/doi/10.1021/acsanm.0c02746.

Detailed schematic illustration of sample fabrication procedure, photographs of samples, spectrum measurement setup diagram, microscopic images of DI water droplet for contact angle measurement, spectrum data plots on CIE1931 color map, and schematic description of liquid sensitive coloration (PDF)

Demonstration video of the discus fish patterned sample immersed in different liquids (MP4)

AUTHOR INFORMATION

Corresponding Authors

Yong-Sang Ryu − *Sensor System Research Center, Korea Institute of Science and Technology, Seoul 02792, Republic of Korea;* orcid.org/0000-0002-3222-4231; Email: ysryu82@kist.re.kr

Seung-Yeol Lee − *School of Electronic and Electrical Engineering, Kyungpook National University, Daegu 41566, Republic of Korea;* orcid.org/0000-0002-8987-9749; Email: seungyeol@knu.ac.kr

Authors

Hee-Dong Jeong − *School of Electronic and Electrical Engineering, Kyungpook National University, Daegu 41566, Republic of Korea*

Jongsu Lee − *Sensor System Research Center, Korea Institute of Science and Technology, Seoul 02792, Republic of Korea; Department of Electrical and Computer Engineering, Seoul National University, Seoul 08826, Republic of Korea*

Eui-Sang Yu − *Sensor System Research Center, Korea Institute of Science and Technology, Seoul 02792, Republic of Korea; Department of Electrical and Computer Engineering, Seoul National University, Seoul 08826, Republic of Korea*

Taehyun Kim − *Sensor System Research Center, Korea Institute of Science and Technology, Seoul 02792, Republic of Korea; Department of Micro/Nano Systems, Korea University, Seoul 02841, Republic of Korea*

In Soo Kim − *Nanophotonics Research Center, Korea Institute of Science and Technology, Seoul 02792, Republic of Korea*

Sin-Doo Lee − *Department of Electrical and Computer Engineering, Seoul National University, Seoul 08826, Republic of Korea;* orcid.org/0000-0003-4550-2955

Complete contact information is available at: https://pubs.acs.org/10.1021/acsanm.0c02746

Author Contributions

H.-D.J. and J.L. contributed equally. The manuscript was written through contributions of all authors. All authors have given approval to the final version of the manuscript.

Notes

The authors declare no competing financial interest.

ACKNOWLEDGMENTS

S.-Y.L. is supported by the National Research Foundation of Korea (NRF) grant funded by the Korea government (MSIT) (nos. 2017R1C1B2003585 and 2020R1A4A1019518). Y.-S.R. acknowledges supports in part by KIST intramural grants (nos. 2V07880 and 2E30140) and NRF grant funded by the Korea government (MSIT) (no. 2020M3H5A1081103). I.S.K. acknowledges support from the National Research Foundation of Korea (NRF) grant funded by the Korea government (MSIT) (no. 2020R1C1C1013474).

ABBREVIATIONS

BEMT, Bruggeman's effective medium theory
FP, Fabry−Perot
FPR, Fabry−Perot resonance
MDM, metal−dielectric−metal
PBVE, perfluoro-(butenyl vinyl ether)
RI, refractive index
RIE, reactive ion etching
RIU, refractive index unit
SEM, scanning electron microscopy
TMM, transfer matrix method

REFERENCES

(1) Sun, J.; Bhushan, B.; Tong, J. Structural coloration in nature. *RSC Adv.* **2013**, *3*, 14862−14889.

(2) Freestone, I.; Meeks, N.; Sax, M.; Higgitt, C. The lycurgus cup - a roman nanotechnology. *Gold Bull.* **2007**, *40*, 270−277.

(3) Dammann, H. Color separation gratings. *Appl. Optics* **1978**, *17*, 2273−2279.

(4) Yablonovitch, E. Inhibited spontaneous emission in solid-state physics and electronics. *Phys. Rev. Lett.* **1987**, *58*, 2059−2062.

(5) Serpe, M. J.; Kang, Y.; Zhang, Q. M. *Photonic Materials for Sensing, Biosensing and Display Devices*, 1st ed.; Springer Series in Materials Science; Springer International Publishing: Cham, 2016; p 1 (XV, 364 pages). https://hdl.loc.gov/loc.gdc/stacks.2019740728.

(6) Kim, J. H.; Moon, J. H.; Lee, S.-Y.; Park, J. Biologically inspired humidity sensor based on three-dimensional photonic crystals. *Appl. Phys. Lett.* **2010**, *97*, 103701−103703.

(7) Landy, N. I.; Sajuyigbe, S.; Mock, J. J.; Smith, D. R.; Padilla, W. J. Perfect metamaterial absorber. *Phys. Rev. Lett.* **2008**, *100*, 207402−207405.

(8) Do, Y. S.; Park, J. H.; Hwang, B. Y.; Lee, S.-M.; Ju, B.-K.; Choi, K. C. Plasmonic color filter and its fabrication for large-area applications. *Adv. Opt. Mater.* **2013**, *1*, 133−138.

(9) Nam, H.; Song, K.; Ha, D.; Kim, T. Inkjet printing based monolayered photonic crystal patterning for anti-counterfeiting structural colors. *Sci. Rep.* **2016**, *6*, 30885−30893.
(10) Nath, N.; Chilkoti, A. A colorimetric gold nanoparticle sensor to interrogate biomolecular interactions in real time on a surface. *Anal. Chem.* **2002**, *74*, 504−509.
(11) Pursiainen, O. L.; Baumberg, J. J.; Winkler, H.; Viel, B.; Spahn, P.; Ruhl, T. Nanoparticle-tuned structural color from polymer opals. *Opt. Express* **2007**, *15*, 9553−9561.
(12) Ji, T.; Peng, L.; Zhu, Y.; Yang, F.; Cui, Y.; Wu, X.; Liu, L.; He, S.; Zhu, F.; Hao, Y. Plasmonic broadband absorber by stacking multiple metallic nanoparticle layers. *Appl. Phys. Lett.* **2015**, *106*, 161107−161111.
(13) Ehlert, O.; Thomann, R.; Darbandi, M.; Nann, T. A four-color colloidal multiplexing nanoparticle system. *ACS Nano* **2008**, *2*, 120−124.
(14) Yu, E.-S.; Lee, S.-H.; Bae, Y.-G.; Choi, J.; Lee, D.; Kim, C.; Lee, T.; Lee, S.-Y.; Lee, S.-D.; Ryu, Y.-S. Highly sensitive color tunablility by scalable nanomorphology of a dielectric layer in liquid-permeable metal-insulator-metal structure. *ACS Appl. Mater. Interfaces* **2018**, *10*, 38581−38587.
(15) Bruggeman, D. A. G. The calculation of various physical constants of heterogeneous substances. I. The dielectric constants and conductivities of mixtures composed of isotropic substances. *Ann. Phys.* **1935**, *416*, 636−791.
(16) Liu, Z.; Liu, X.; Huang, S.; Pan, P.; Chen, J.; Liu, G.; Gu, G. Automatically acquired broadband plasmonic-metamaterial black absorber during the metallic film-formation. *ACS Appl. Mater. Interfaces* **2015**, *7*, 4962−4968.
(17) Kim, S.-J.; Choi, H.-K.; Lee, H.; Hong, S.-H. Solution-processable nanocrystal-based broadband Fabry−Perot absorber for reflective vivid color generation. *ACS Appl. Mater. Interfaces* **2019**, *11*, 7280−7287.
(18) Lee, I.-H.; Lee, S.-H.; Keum, C.-M.; Kim, S.-U.; Lee, S.-D. Combinatorial color arrays based on optical micro-resonators in monolithic architecture. *Opt. Express* **2014**, *22*, 15320−15327.
(19) Lee, I.-H.; Yu, E.-S.; Lee, S.-H.; Lee, S.-D. Full-coloration based on metallic nanostructures through phase discontinuity in Fabry-Perot resonators. *Opt. Express* **2019**, *27*, 33098−33110.
(20) Kim, T.; Yu, E.-S.; Bae, Y.-G.; Lee, J.; Kim, I. S.; Chung, S.; Lee, S.-Y.; Ryo, Y.-S. Asymmetric optical camouflage: tuneable reflective colour accompanied by the optical Janus effect. *Light: Sci. Appl.* **2020**, *9*, 175.
(21) Jang, J.; Badloe, T.; Yang, Y.; Lee, T.; Mun, J.; Rho, J. Spectral modulation through the hybridization of Mie-scatterers and quasi-guided mode resonances: realizing full and gradients of structural color. *ACS Nano* **2020**, *14*, 15317−15326.
(22) Qiu, Y.; Yang, S.; Sheng, K. Photolithographic patterning of cytop with limited contact angle degradation. *Micromachines* **2018**, *9*, 509−518.
(23) Cai, W.; Shalaev, V. M. *Optical Metamaterials*; Springer, 2010; Vol. *10*.

https://dx.doi.org/10.1021/acsanm.0c02746
ACS Appl. Nano Mater. 2021, 4, 389−395